RSC Advances

PAPER

View Article Online
View Journal | View Issue

Cite this: *RSC Adv.*, 2023, **13**, 23659

The potentials of boron-doped (nitrogen deficient) and nitrogen-doped (boron deficient) BNNT photocatalysts for decontamination of pollutants from water bodies

Yahaya Saadu Itas, *[a] Kamaluddeen Abubakar Isah,[a] Awwal Hussain Nuhu,[a] Razif Razali,[b] Salisu Tata,[a] Naseer K. A.,[c] Abubakr M. Idris,[de] Md. Habib Ullah[f] and Mayeen Uddin Khandaker *[gh]

This work investigates the structural, elastic, electronic, and photoabsorption properties of boron- (N-deficient) and nitrogen- (B-deficient) doped single-walled boron nitride nanotube (SWBNNT) for photocatalytic applications for the first time. All calculations of the optimized systems were performed with DFT quantum simulation codes. The results of the structural analysis showed that SWBNNT is stable to both B and N dopants. It was also observed that the photodecomposition activity of the B-doped nanotube improved significantly under the condition of slight compressive stress, while it decreased for the N-doped nanotube. Therefore, N-doped SWBNNT showed poor performance under external pressure. Both B and N-doped systems could narrow the wide band gap of SWBNNT to the photocatalytic region below 3 eV, therefore this material can be used as photocatalysts in water splitting for hydrogen evolution, dye degradation, wastewater treatment, *etc.* Analysis of the optical properties revealed that B-doped SWBNNT absorbs more photons in the visible range than the N-doped SWBNNT and can therefore be considered as a more efficient photocatalyst. In addition, it was found that all doped nanotubes are anisotropic since the absorption in one direction of nanotube axes is worse than the other.

Received 8th June 2023
Accepted 23rd July 2023

DOI: 10.1039/d3ra03838f

rsc.li/rsc-advances

1. Introduction

Environmental pollution is one of the key global challenges that seriously threatens the health of our ecosystem. In order to get rid of these problems including the decontamination of water bodies, various efforts have been made to develop efficient, inexpensive and environmentally friendly technologies.[1] Photocatalysis is one of the most promising methods to control pollution and water degradation.[2] Previously, several investigations were made using different materials as photocatalysts for the purpose of decomposition of waste and organic materials. The whole process involves oxidation and reduction reactions that facilitate the absorption of photons under visible light.[3] Photocatalysis become popular because the traditional treatment techniques, which rely heavily on centralized systems, are no longer a sustainable technology. It has been reported that transition metal oxides have been the most widely used photocatalysts for wastewater treatment because of their high photocatalytic activity and excellent solubility.[4] Despite the successes that have been achieved by using various materials as photocatalysts, problems regarding the efficient, inexpensive, mechanically stable, and thermally stable photocatalysts remain. Some of the photocatalysts are unable to absorb photons for a long time, and others lack thermal stability at high temperatures due to exposure to sunlight, *etc.* In addition, other photocatalysts absorb photons in the ultraviolet region, which accounts for only 3% of solar radiation, and therefore need to be adjusted. As an example, when Au-doped TiO_2 photocatalysts were used for dye degradation, they showed 70% photoactivity in degrading dye pollutants under UV irradiation and only 30% under sunlight.[5] Another problem associated with TiO_2 photocatalysts is that most of the activated charge carriers recombine before reaching the surface, preventing interactions

[a]*Department of Physics, Bauchi State University, Gadau, PMB 65, Gadau, Bauchi, Nigeria. E-mail: yitas@basug.edu.ng*

[b]*Department of Physics Faculty of Science, Universiti Teknologi Malaysia, Malaysia*

[c]*Department of Physics, Farook College (Autonomous), Kozhikode, 673632, India*

[d]*Department of Chemistry, College of Science, King Khalid University, Abha 62529, Saudi Arabia*

[e]*Research Center for Advanced Materials Science (RCAMS), King Khalid University, Abha 62529, Saudi Arabia*

[f]*Department of Physics, American International University-Bangladesh (AIUB), 408/1, Kuratoli, Khilkhet, Dhaka 1229, Bangladesh*

[g]*Centre for Applied Physics and Radiation Technologies, School of Engineering and Technology, Sunway University, Bandar Sunway 47500, Selangor, Malaysia. E-mail: mu_khandaker@yahoo.com*

[h]*Faculty of Graduate Studies, Daffodil International University, Daffodil Smart City, Birulia, Savar, Dhaka 1216, Bangladesh. E-mail: mayeenk@diu.edu.bd*

with the absorbed molecules. This clearly indicates the necessity of exploring new materials having suitable physicochemical properties for efficient photocatalytic applications.

Nowadays, boron nitride nanotubes (BNNTs) are gaining popularity due to their versatile properties such as low density, high surface area, good mechanical strength, high thermal stability, *etc.*[6] Being a wide bandgap (4–6 eV) semiconductor, BNNTs have always been in demand for numerous applications in electronic devices such as p–n junctions, TFTs (thin film transistors) and transparent contacts. Moreover, they have been used in applications such as the reinforcement of polymers, ceramics and metals, sensors, *etc.*[7] However, the reported larger band gap (4 eV to 6 eV)[8] of BNNTs across all chirality reduced their potential for photocatalysis applications. Therefore, for perfect absorption under visible light, it is necessary to decrease their band gap below 3 eV. BNNTs have been used as electrolytes for CO_2 reduction and have been shown to be excellent with a cut-off potential of −0.96 eV.[9] However, a search of the literature reveals that the photocatalytic potential of single-walled boron nitride nanotubes (SWBNNTs) has not been reported yet. In this work, we studied the potential of SWBNNTs as candidates for photocatalysis for the decontamination of pollutants from water bodies. This has been performed by independent doping of boron (N-deficient SWBNNT) and nitrogen (B-deficient SWBNNT) atoms using popular density functional theory. The SWBNNT was chosen for this research because of its versatile thermal, mechanical, electronic and optical properties. Their high aspect ratio (large surface area) makes them well-absorbing surfaces, allowing large amounts of solar radiation to be absorbed in a relatively short time. In this study, the B-doped, N-deficient SWBBNT photocatalyst is obtained by replacing one atom of B with one atom of N. On the other hand, the N-doped, B-deficient SWBNNT is obtained by replacing one B atom with one N atom. This work considered DFT analysis as a tool to determine the properties of the investigated system because DFT gives the accurate prediction of material properties for unknown systems without the knowledge of any experimental input. It also helps to understand how these nanotubes behave and operate under different conditions before being subject to any practical or experimental tests.

2. Research methods

The detailed models of the study include pristine SWBNNT, B-doped SWBNNT, and N-doped SWBNNT systems. The doping was carried out with 3.1% each of B and N atoms. The original structure of the SWBNNT was optimized using the default bond length of 1.45 according to the experimental data.[10] The analysis of the structural and elastic properties of the studied systems was performed using the Murnaghan equation of state, which describes the relationship between the volume of the pristine and N-doped systems and the tensile pressure.[11]

$$S(V) = \frac{K_0}{K'_0}\left[\left(\frac{V}{V_0}\right)^{-K'_0} - 1\right] \quad (1)$$

where $\frac{V}{V_0}$ is the reduction in the volume of the nanotubes under stress and $\frac{K_0}{K'_0}$ is the reduction of the force constant under stress. All calculations regarding electronic interactions were done using the generalized gradient approximation (GGA) method in terms of the Perdew–Burke–Ernzerhof (PBE) exchange–correlation functional.[12] To ensure accurate results, good convergence and balance between computational cost and accuracy, a kinetic energy cut-off value of 65 Ry was used while *k*-point sampling of 1 × 1 × 40 was used in the gamma point of the Brillouin zone. The optical properties of the interacting systems were calculated using the imaginary dielectric function based on the Kramers–Kronig relations[7]

$$\varepsilon_2 = -\frac{2\omega}{\pi} P \int_0^{\infty} \frac{\varepsilon_1(\omega') - 1}{\omega'^2 - \omega^2} \mathrm{d}\omega' \quad (2)$$

Furthermore, because this research is chirality-specific, it does not consider the length of the SWBNNT. Only one unit cell of SWBNNT (7, 7) which contains 28 atoms has been utilized in this study. Due to its fixed chirality, the length of the nanotube remains constant throughout the process.

3. Results and discussion

3.1 Structural and elastic properties

The basis of the efficiency of a photocatalytic material lies in its ability to recover its size and shape after partial elastic deformation by solar radiation. On this basis, photocatalysts with high tensile stress, Young's modulus and shear modulus are required for perfect photon absorption. On the other hand, photocatalysts that exhibit lower values of Young's modulus, surface-to-volume ratio, and low shear stress are not efficient in photoabsorption.[13] As part of this work, we have investigated the structural and elastic properties of the systems under investigation and analyzed the results accordingly. Table 1 shows the calculated results of the formation energy distribution of the three systems examined. This table showed that the original SWBNNT system was stable to both B and N atom doping. However, an increase in the diameter of the SWBNNT was observed upon doping with B atoms due to the relatively larger diameter of B compared to the N atom. On the other hand, a slight decrease in the diameter of the SWBNNT was observed due to the N-doping in the original system. The formation energy was higher in the B-doped system than in the N-doped SWBNNT. Fig. 1(a)–(c) show the optimized structure of the studied photocatalysts. The mechanical properties of the examined systems were first analyzed by calculating the respective bulk modulus in each case. Relative to the pristine SWBNNT, a bulk modulus of 967.83 GPa was obtained, which agreed well with the theoretical and experimental values obtained.[14] The obtained bulk moduli for B-doped and N-doped SWBNNTs are 968.45 GPa and 968.32 GPa, respectively, indicating that the B-doped SWBNNT is mechanically more stable than the pristine and N-doped SWBNNT systems. In addition, the obtained result

Table 1 Formation energy distribution of the SWBNNT photocatalysts

Material	Substitution	Formation energy (eV)	Diameter (nm)
Pristine SWBNNT	No substitution	−429.60	14.94
B-doped SWBNNT	N atom	−415.85	15.08
N-doped SWBNNT	B atom	−442.19	14.80

also showed that the bulk modulus does not depend on the diameter of the interacting system.

The effects of the total energy on the volume of the examined systems were studied and analyzed. The calculated results are shown in Fig. 2(a)–(c). In all cases, the total energy was observed to vary directly with the volume and then reversed after reaching the most equilibrium volumes of the studied nanotubes. Fig. 2(a) shows the variation of total energy with the volume of the pristine SWBNNT semiconductor. The system showed the largest equilibrium volume of 1300 $Å^3$, which corresponds to a total energy of −974.77 eV. This is the optimal volume to achieve the overall optimized energy of the system. In addition, this is the region where the electron–hole interactions predominate over the nucleus–nucleus interactions. The calculated equilibrium volume of the B-doped and N-doped SWBNNTs was 1300.46 $Å^3$ and 1298.62 $Å^3$ as shown in Fig. 2(b) and (c), respectively. The blue shift in the volume of the B-doped SWBNNT was due to the increased diameter of the doped system, while the red shift in the N-doped system was due to the decrease in the diameter of the doped system, as obtained in previous sections. Furthermore, the inverse variations in total energy with volume were due to repulsive forces, while the obtained direct variations in total energies were due to attractive forces.[15] In terms of bond lengths, Fig. 2(d) shows that the closest distance between B–N or B–B atoms is 1.46 Å, which agrees with results from other studies.[16] Furthermore, the obtained total energy corresponding to this bond length has the same value of −974.77 eV as in Fig. 2(a). Therefore, all obtained parameters of the pristine SWBNNT can be matched to each other. The bond length values obtained for the B-doped and N-doped SWBNNTs are 1.47 Å and 1.452 Å, respectively (Fig. 2(e) and (f)), which are all in the range of reported experimental values for BNNTs. Based on these results, the N-doped SWBNNT is considered stronger because of the shortened bond length, while the native SWBNNT is considered less strong because of the increased bond length. To justify this, it was found that the calculated values of the bond lengths of all systems studied were inversely related to the bond order. Therefore, strong bond orders are accompanied by strong attractive forces that hold the interacting atoms together.

The external pressure (stress) produces a significant effect on the photocatalytic activities of materials. Materials that undergo higher compressions perform no photocatalytic activity.[17] It is therefore necessary to investigate the materials' response to external stress before being imported for photocatalysis. For the purpose of this work, we have evaluated the effects of tensile pressure (stress) on the volumes of the pristine, B-doped and N-doped SWBNNT structures. External pressure varies inversely with volumes for all the studied systems, which is consistent with the theoretical findings.[18] The calculated optimum stress obtained for pristine SWBNNT is 5.23 GPa as shown in Fig. 3(a). Fig. 3(b) revealed that the B-doped SWBNNT photocatalyst withstands more tensile pressure than the pristine SWBNNT due to stronger bond energies. It has been observed that the photodecomposition activity of the B-doped (3.1%) nanotube improved clearly when slight compressive stress was applied, whereas the photodecomposition activity was degraded for the N-doped (3.1%) nanotube. Therefore, N-doped SWBNNT presented in Fig. 3(c) demonstrated weak performance under external pressure. Fig. 3(d)–(f) show the analysis of the calculated Young's moduli of the investigated nanotubes with different lengths. The N-doped SWBNNT proved to be stiffer due to the shorter bond length, while pure SWBNNT showed lower stiffness due to the longer bond length. To summarize our findings, Table 2 presents the calculated optimization parameters of the three systems studied. From the table, it can be observed that doping significantly improved the mechanical

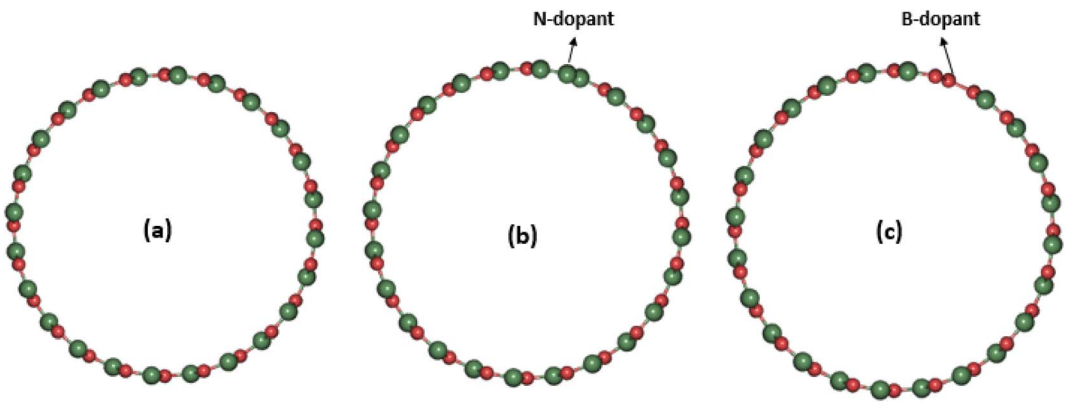

Fig. 1 Geometrical structures of (a) pristine SWBNNT, (b) N-doped SWBNNT and (c) B-doped SWBNNT. The red ball represents boron atoms while the green ball represents nitrogen atoms.

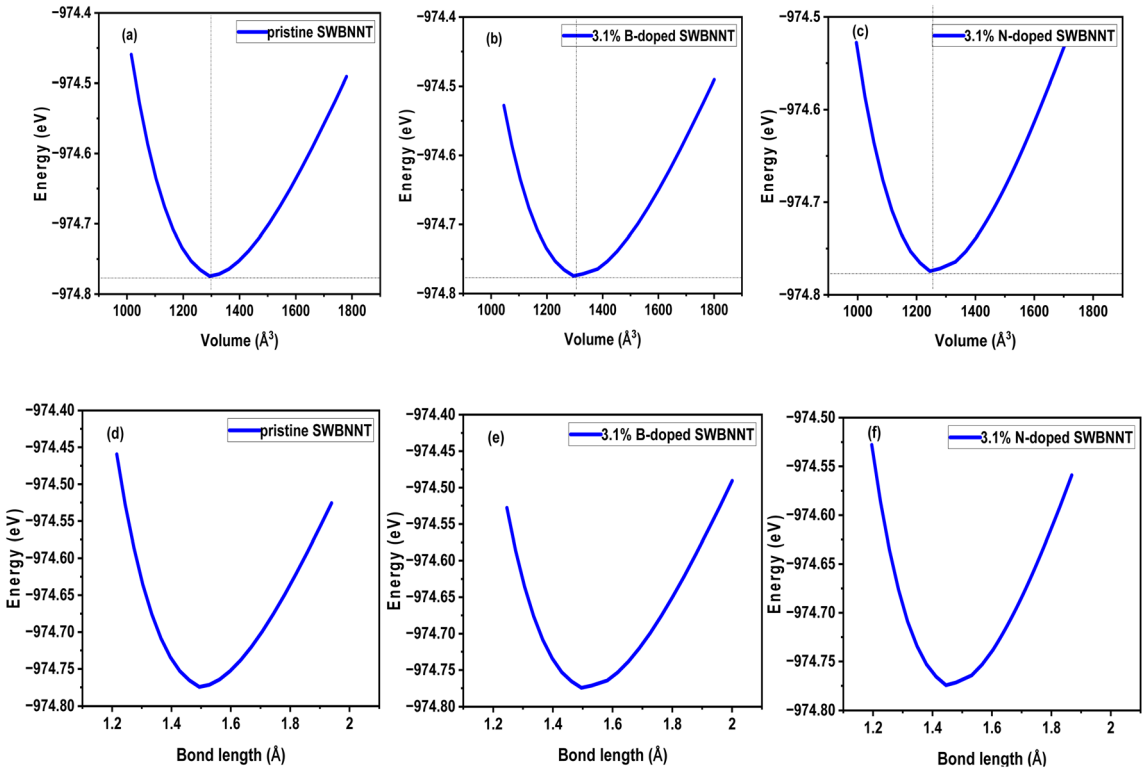

Fig. 2 Variation of energy with volumes of (a) pristine SWBNNT (b) B-doped (3.1%) SWBNNT and (c) N-doped (3.1%) SWBNNT. Energy variation with bond lengths of (d) pristine SWBNNT (e) B-doped (3.1%) SWBNNT and (f) N-doped (3.1%) SWBNNT.

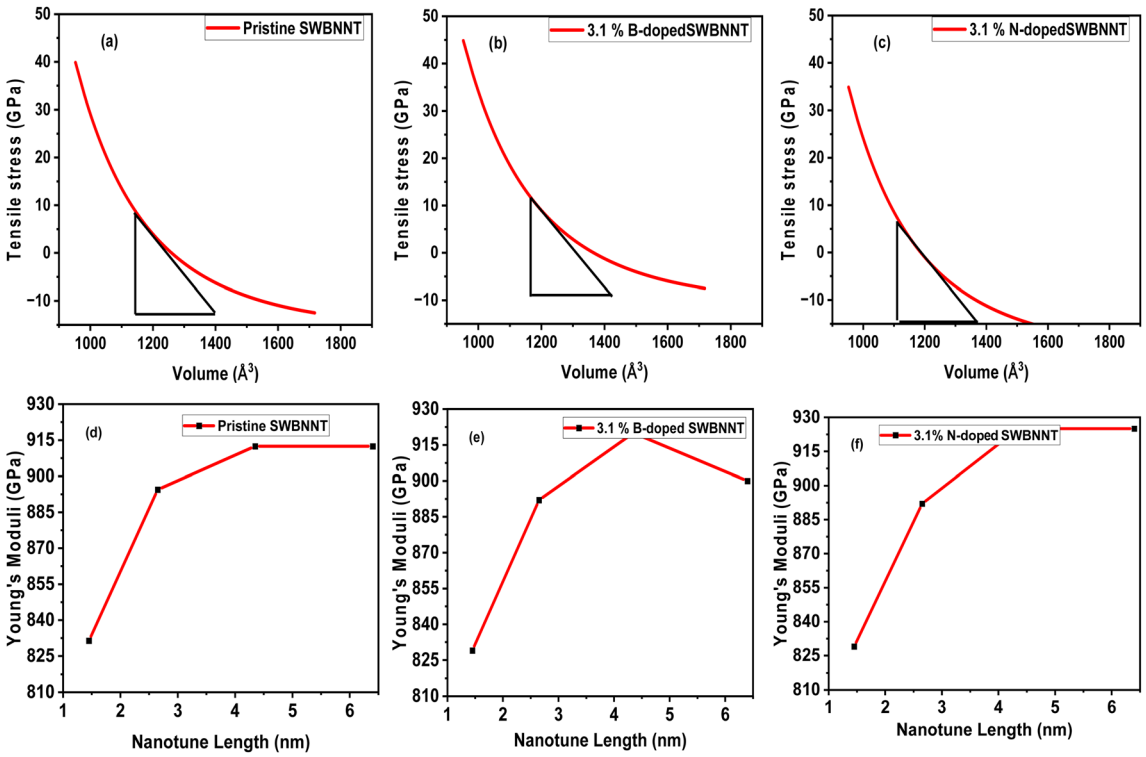

Fig. 3 Variation of tensile pressure with volumes of (a) pristine SWBNNT (b) B-doped (3.1%) SWBNNT and (c) N-doped (3.1%) SWBNNT. Young's moduli with nanotube lengths of (d) pristine SWBNNT (e) B-doped (3.1%) SWBNNT and (f) N-doped (3.1%) SWBNNT.

Table 2 Calculated elastic parameters of the investigated systems

Material	Bond length (Å)	Bond energy (eV)	Volume $(a.u)^3$	Stress (GPa)	Young's modulus (GPa)
Pristine SWBNNT	1.46	−974.77	1300.00	5.23	918.32
B-doped (3.1%) SWBNNT	1.47	−974.75	1300.46	5.35	921.91
N-doped (3.1%) SWBNNT	1.45	−974.76	1298.62	5.03	928.03

states and structural stability of the SWBNNT nanotube which fit it to be imported as a better candidate for photocatalysis under visible light.

3.2 Electronic properties

The efficient performance of photocatalysts under visible light strongly depends on their electronic structure and band gap energy. For the purpose of optimum performance, the band gap should be less than 3 eV in order to extend the photoabsorption into the visible range and thus use solar energy efficiently. Furthermore, in the water splitting technique, the energy must be in the range of 2.2 eV to 2.8 eV and this exceeds the free energy of water splitting (1.23 eV).[19] In this work, we first analyze the electronic band structure of the pristine SWBNNT semiconductor, and the results are shown in Fig. 4(a). The calculations were performed with GGA implemented in Kohn–Sham DFT and G_0W_0 approximation methods. The results of the GGA showed a band gap of 3.3 eV. Furthermore, it has been observed that both the valence band maxima and the conduction band minima have the same momentum, hence the band gap is direct, favoring the emission of light during electron–hole recombination. However, due to the reported underestimation of the bandgap by GGA, we performed the calculations again using the G_0W_0 approximation. G_0W_0 was chosen because it provides an accurate description of the electronic properties of many-body systems. The calculated bandgap of the pristine SWBNNT obtained with the G_0W_0 method was 5.6 eV, which agrees with the obtained experimental results. Therefore, SWBNNT in its current state is not suitable for use as a photocatalyst, since the obtained band gap is much higher than 3 eV and therefore it cannot absorb a photon in the visible range. To tune it for possible photocatalysis, we have successfully narrowed the band gap *via* independent doping of B (3.1%) and N (3.1%) atoms respectively. Fig. 4(b) and (c) present the calculated electronic band gaps of B-doped and N-doped SWBNNTs with 3.1% dopant concentrations. The SWBNNT doped with B atom demonstrated an indirect band gap of 2.4 eV which is less than 3 eV, and hence can be a better photocatalyst. Additionally, B-doped SWBNNT releases heat during electron–hole recombination. The obtained band gap of N-doped SWBNNT was found to be 2.56 eV which also agrees with the experimental range for photocatalysts. In order to determine the degree to which the energy levels are occupied by electrons, we analyzed the electronic density of states for all systems examined. As shown in Fig. 5(a), SWBNNT showed a uniform distribution of energy states in both the conduction band and the valence band, while showing empty states from −5 eV to 1.8 eV. As shown in Fig. 5(b) and (c), the probability of finding electrons at the Fermi level is higher for the B-doped and N-doped SWBNNTs than for the pristine SWBNNTs. Therefore, the band gaps in the doped systems are smaller, indicating the involvement of dopants. In addition, more energy states appeared in the doped systems below −7.5 eV due to the occupation of spaces by dopants.

The photocatalytic activities of nanotubes are similarly enhanced by surface hybridization, particularly in environmental remediation and energy conversion. To analyze this, we investigated different orbital participation for narrowing the

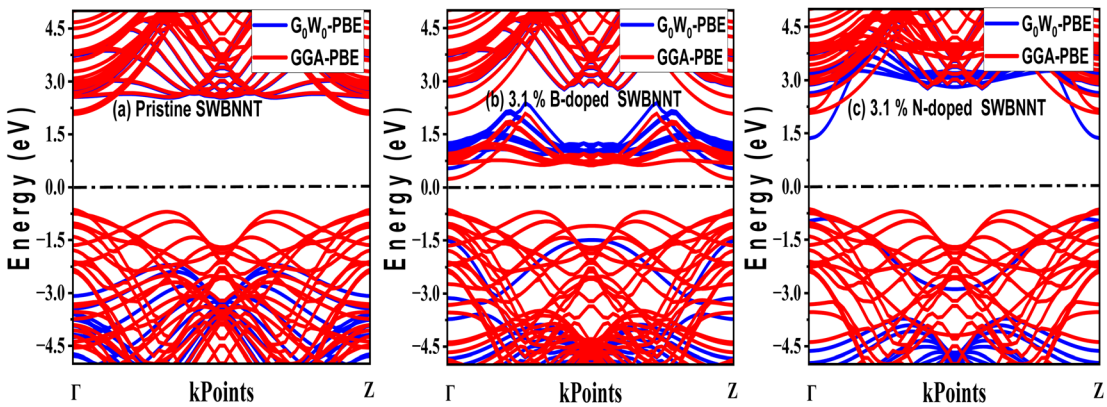

Fig. 4 Electronic band structures of (a) pristine SWBNNT (b) B-doped SWBNNT and (c) N-doped SWBNNT.

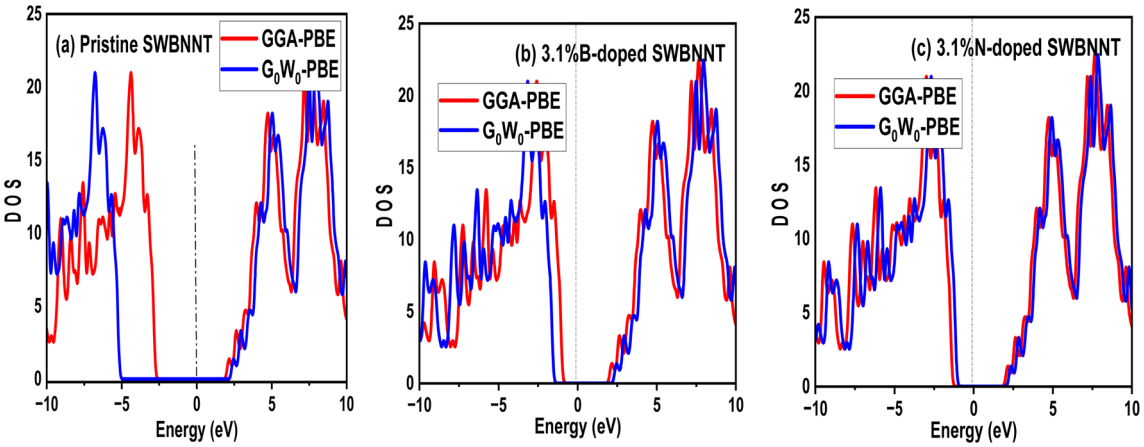

Fig. 5 Electronic density of states of (a) pristine SWBNNT (b) B-doped SWBNNT and (c) N-doped SWBNNT.

band gap in SWBNNT up to the photocatalytic regime. Fig. 6(a) shows the partial density of states (PDOS) for B-doped SWBNNT, while Fig. 6(b) shows the PDOS for N-doped SWBNNT. In each case, p orbitals of B and N atoms of the pristine SWBNNT were observed with no contributions near the Fermi level. While p orbitals of B and N dopants occupied higher states near the Fermi level in the valence band. Furthermore, it can be seen that the p orbital of the N-doped SWBNNT extends to the conduction band, so the properties of the doped SWBNNT photocatalyst were determined by the p orbitals of the dopant atoms.

Factors affecting the photoperformance of the photocatalyst include vacancies, dopant concentration, electron–hole recombination, and so on. For some materials, the bandgap increases with vacancy, while for some other materials, the bandgap decreases due to vacancy. In terms of dopant concentration, we analyzed the effects of B and N dopant concentrations on the electronic band gap of pristine SWBNNT. Interestingly, both systems showed an inverse relationship with the band gap. Fig. 7(a) shows the Fermi level closure when 9.37% B impurities were used to dope a unit cell of SWBNNT. In the case of N-type doping, Fig. 7(b) shows a very narrow band gap of 0.86 eV when SWBNNT was doped with 6.25% N impurities. Furthermore, it was confirmed that the optimum concentration of B and N atoms for perfect photoabsorption under visible light is obtained when a dopant concentration of 3.1% is used per unit cell of SWBBNT.

3.3 Optical absorptions

Light absorption and scattering play a significant role in the overall process of photocatalysis, especially in the choice of suitable catalysts besides other physical parameters. The efficiency rate of photocatalysts depends on their light absorption properties which are dependent on the imaginary dielectric constant.[20] We define the optical response of photocatalyst materials to the incident solar radiation in terms of the real and imaginary dielectrics as[21]

$$\varepsilon(\omega) = \varepsilon_1(\omega) + \varepsilon_2(\omega) \quad (6)$$

where $\varepsilon_1(\omega)$ is the real part and $\varepsilon_2(\omega)$ is the imaginary part of the optical dielectric constant. The real part of the dielectric function takes care of the photon energy dispersion, while the imaginary part of the dielectric function describes the photon

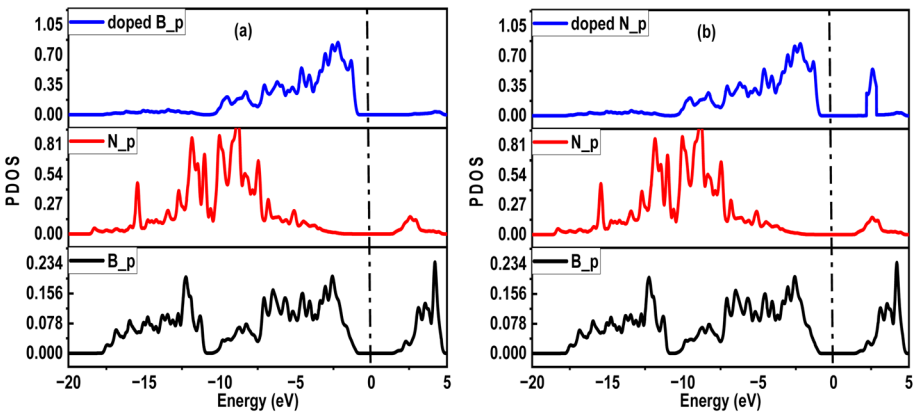

Fig. 6 PDOS diagrams of (a) B-doped SWBNNT (b) N-doped SWBNNT.

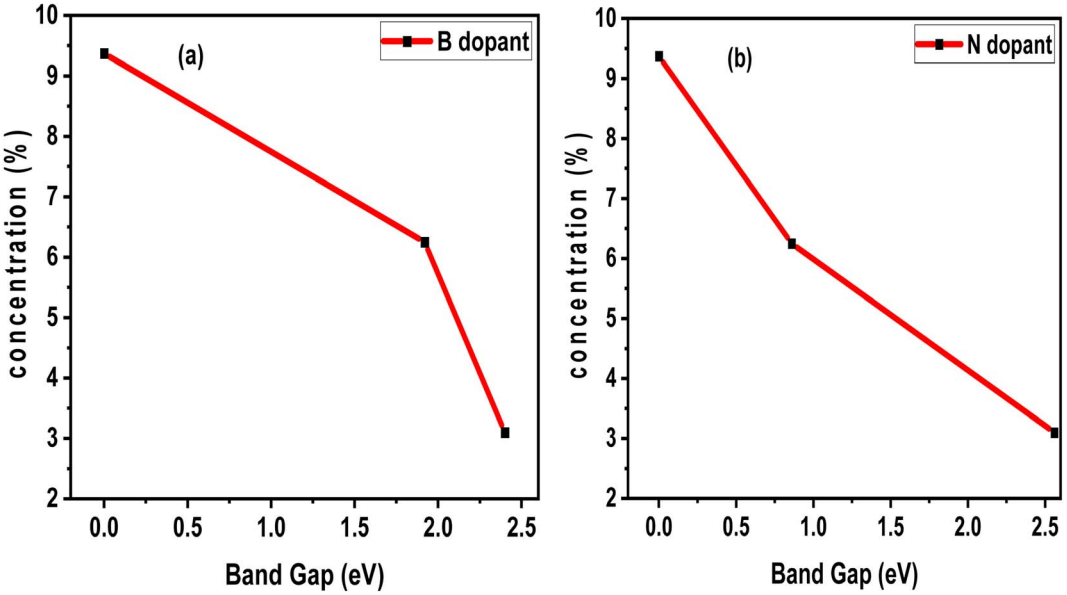

Fig. 7 Effects of dopant concentration (a) B dopant (b) N dopant.

energy absorption. The photoabsorption potentials of the SWBNNT, B-doped SWBNNT, and N-doped SWBNNT semiconductors were investigated in both parallel and perpendicular directions of the respective nanotube axis. Fig. 8(a) shows the intensity of the energy absorbed by the pristine SWBNNT in terms of the imaginary dielectric function. The observed optical band gap shows the highest imaginary intensity of 4.8 eV, also the highest peak at this point shows high energy absorption.

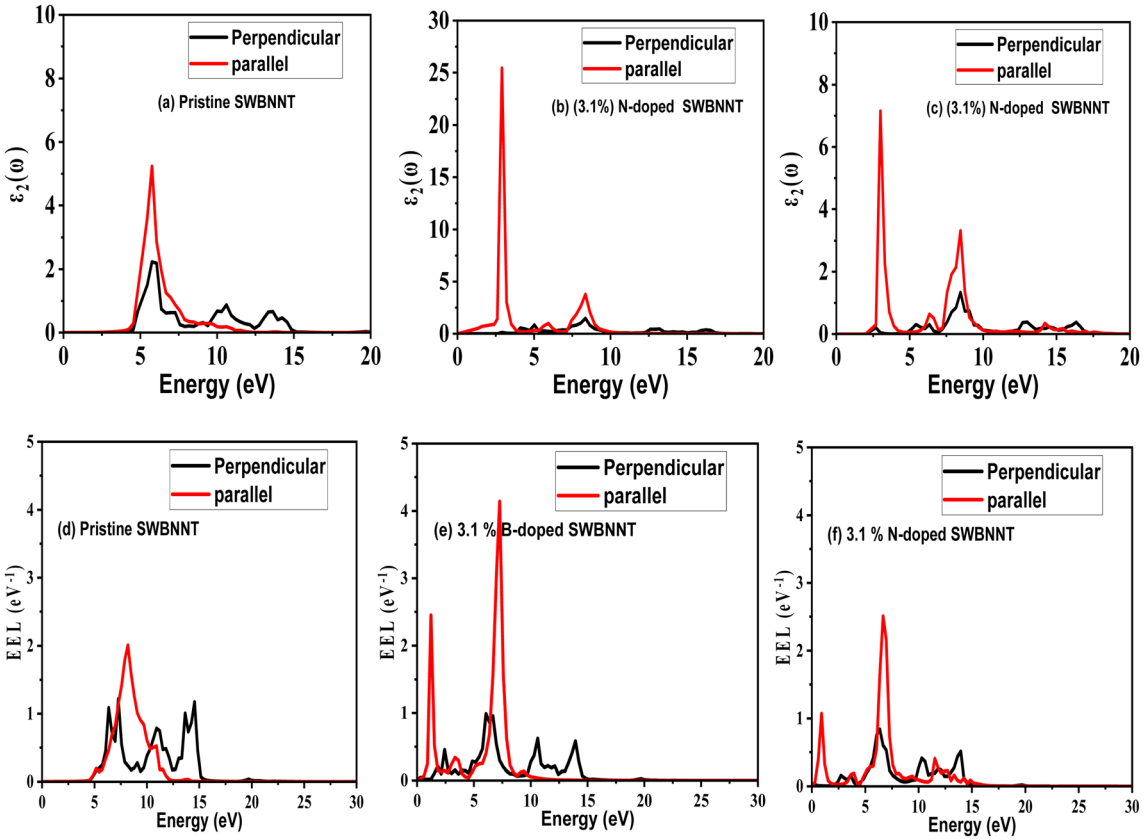

Fig. 8 Imaginary dielectric (absorption) spectra of (a) pristine SWBNNT, (b) B-doped SWBNNT and (c) N-doped SWBNNT. EELS spectra of (d) pristine SWBNNT, (e) B-doped SWBNNT and (f) N-doped SWBNNT.

Table 3 Photoabsorption properties of the investigated systems

Material	Optical bandgap	ε_2 (visible)	ε_2 (ultraviolet)	Remark
Pristine SWBNNT	5.6	5.72	2.10	Inefficient
B-doped SWBNNT	2.61	25.42	3.78	Very efficient
N-doped SWBNNT	2.7	7.15	3.32	Efficient

However, the absorbed energy lies in the shortwave range up to the ultraviolet range. Additionally, only 3% of sunlight can be absorbed in the UV region, so this SWBNNT needs to be fine-tuned to less than 3 eV to be able to absorb the light in the visible region. In Fig. 8(b), two peaks were observed in the visible and UV ranges respectively. Compared to pure SWBNNT, B-doped SWBNNT showed perfect absorption in the longer wavelength range. An optical bandgap of 2.61 eV was obtained, which corresponds to an imaginary dielectric intensity of 26.43. The material also absorbs small amounts of photons in the UV range. This, together with the high absorption in the visible region, B-doped SWBNNT turned out to be a better candidate for photocatalysis such as hydrogen evolution by water splitting, biodegradation, and wastewater purification. Photocatalytic behavior was also observed for N-doped SWBNNT as shown in Fig. 8(c). However, this system showed lower absorption than the B-doped system in the visible range and higher absorption than the B-doped system in the UV range. In addition, both B-doped and N-doped systems showed poor absorption in the perpendicular direction, indicating that the B-doped and N-doped SWBNNT photocatalysts are anisotropic and this conforms to the observed characteristics of nanotube materials.[22]

It has been reported that materials that absorb more light lose less energy.[23] To examine our systems, we performed an electron energy loss analysis (EELS) of the pristine, B-doped and N-doped SWBNNTs. Fig. 8(d) shows the calculated EELS spectra of pristine SWBNNT. This system showed no electromagnetic interactions below 4.9 eV. In this range, the material neither absorbs nor loses energy. The energy losses observed for this material were highest in the UV range and lowest in the radio wave range, meaning that it absorbs more energy in the radio wave range than in the UV range. Concerning B-doped SWBNNT, shown in Fig. 8(e), complete interactions can be seen in both the visible, UV, and radio wave regimes. The lowest energy loss was observed at 2.6 eV, which corresponds to the highest absorption by the same material previously reported in Fig. 8(b), and this agrees well with the inverse relationship between energy loss and energy absorption.[24] Compared to N-doped SWBNNT, Fig. 8(f) showed a relatively high energy loss as B-doped SWBNNT, occurring at 2.61 eV. Therefore, this material absorbs less energy in the visible range than B-doped SWBNNT. In addition, greater electron energy loss in the UV region showed that both B-doped and N-doped systems absorb less energy in this region. It can also be observed that all systems studied showed poor electromagnetic interaction in the direction perpendicular to the nanotube axes, confirming the one-dimensional nature, anisotropy and length-to-*d*-axis.

A detailed overview of the calculated photoabsorption parameters of the investigated systems is presented in Table 3, while Table 4 presents various literature results in comparison to the present work. Table 3 shows the highest efficiency with the B-doped SWBNNT due to the highest value of ε_2 in the visible region. The photocatalytic performance of B-doped SWBNNT can be compared to that of the CNT–TiO_2 nanocomposite photocatalyst as shown in Table 4. However, the CNT–TiO_2 nanocomposite cannot be applied to other fields due to its critical band gap, unlike the B-doped SWBNNT, which can be applied to many fields as it can absorb a wide range of the visible spectrum. For the kinetics of photocatalytic processes to be satisfied, the arrangement of band edges and overpotentials with reference to the redox potential must be satisfied. An overpotential is a suitable edge location in eV which is a prerequisite for photocatalytic applications. To reveal the potential application of our studied system, Table 5 presents the calculated experimental value of overpotentials for various photocatalytic applications. Based on the information obtained from the table and compared to the calculated band gap of B-doped SWBNNT photocatalyst, the obtained band gap of this system was found to be 2.61 eV which is greater than the experimental and theoretical overpotential values of 1.8–2 eV (for hydrogen evolution), 1.8 eV (for dye degradation) and 1.95 eV for waste water treatment. Based on this information, it can be mentioned that the investigated B-doped SWBNNT

Table 4 Literature compared

Photocatalyst	Band gap (eV)	ε_2 (visible)	Application	Reference
TiO_2 doped with 5% B	2.4	22.04	Photodegradation	25
CNT–TiO_2 nanocomposite	2.2	25.21	CO_2 reduction and water splitting	26
Sr-doped ZnO/CNT	2.3	19.21	Hydrogen evolution	27
CNT/TiO_2/ZnO	3.2	7.27	Not reported	28
B-doped SWBNNT	2.61	25.42	Photodegradation, wastewater treatment, hydrogen evolution	This work

Table 5 Summary of experimental and theoretical overpotential values for various photoabsorption applications

Experimental overpotential value (eV)	Theoretical overpotential value (eV)	Photocatalytic applications	Reference
1.8–2.0	1.23	Hydrogen evolution by water splitting	29
1.8	1–1.8	Solar cell, dye degradation	30 and 31
1.95	2.0	Photocatalytic waste water treatment, CO_2 capture, hydrogen storage	32 and 33

photocatalyst can be a good candidate for hydrogen production, waste water treatment and dye degradation.

4. Conclusions

In this study, the photocatalytic properties of SWBNNT semiconductors were investigated for the first time on the basis of the independent introduction of extra boron and nitrogen atoms. All the investigated systems were optimized using the PBE exchange functional as implemented in DFT codes. Studies of the structural and elastic properties of all the systems revealed very good stability after independent doping of boron and nitrogen atoms. Based on the analysis of the stress volume relationship, the N-doped SWBNNT demonstrated weak performance under external pressure. Calculation of the electronic behaviors of the SWBNNT under B and N impurities transformed the wider band gap of SWBNNT from 5.6 eV down to a photocatalytic range of 2.61 eV and 2.7 eV respectively. Additionally, the probability of finding electrons at the Fermi level is higher for the B-doped and N-doped SWBNNTs than for the pristine SWBNNTs. In terms of photon absorptions, B-doped SWBNNT showed perfect absorption in the longer wavelength range. An optical bandgap of 2.61 eV was obtained, which corresponds to an imaginary dielectric intensity of 26.43. The material also absorbs small amounts of photons in the UV range. This, together with the high absorption in the visible region, B-doped SWBNNT turned out to be a better candidate for photocatalytic applications such as water splitting, biodegradation, and wastewater purification. In addition, both B-doped and N-doped systems showed poor absorption in the perpendicular direction of nanotube axes, indicating that the B-doped and N-doped SWBNNT photocatalysts are anisotropic and this conforms to the observed characteristics of nanotube materials.

Data availability

All data are available in the manuscript.

Author contributions

Conceptualization, Y. S. I. and M. U. K.; methodology, Y. S. I. and R. R.; software, Y. S. I., R. R., M. H. U. and S. T.; formal analysis, Y. S. I., R. R., K. A. N., and S. T.; resources, R. R. and A. M. I.; data curation, M. U. K. and Y. S. I.; writing—original draft preparation, Y. S. I.; writing—review and editing, M. U. K.; visualization, M. U. K., S. T., K. A. N., M. H. U. and A. M. I. All authors have read and agreed to the published version of the manuscript.

Conflicts of interest

All authors declare no conflicts of interest.

Acknowledgements

The authors acknowledge Bauchi State University, Gadau and Tertiary Education Trust Fund (TETFund) and other institutions who facilitated this through various means including the provision of research tools. The authors extend their appreciation to the Deanship of Scientific Research at King Khalid University for funding this work through a small group Research Project under grant number RGP1/120/44.

References

1 N. Mohammed, A. Aslam, M. Abdullah and K. Jae, Exploring Rapid Photocatalytic Degradation of Organic Pollutants with Porous CuO Nanosheets: Synthesis, Dye Removal, and Kinetic Studies at Room Temperature, *ACS Omega*, 2021, **6**, 2601–2612.
2 T. Gupta and R. P. Chauhan, Photocatalytic degradation of water pollutants using II–VI semiconducting catalysts: a comprehensive review, *J. Environ. Chem. Eng.*, 2021, **9**, 106734.
3 R. Cauwenbergh and S. Das, Photocatalysis: A Green Tool for Redox Reactions, *Synlett*, 2022, **33**, 129–149.
4 A. Krishnan, S. Anna, D. Das, M. Krishnan, V. S. Saji and S. M. A. Shibli, A review on transition metal oxides based photocatalysts for degradation of synthetic organic pollutants, *J. Environ. Sci.*, 2024, **139**, 389–417.
5 P. Silija, N. Binitha, Y. Zahira and M. T. Siti, Au/TiO2 Reusable Photocatalysts for Dye Degradation, *Int. J. Photoenergy*, 2013, **2013**, 752605.
6 Y. S. Itas, B. S. Abdussalam, E. N. Chifu, R. Razif and M. U. Khandaker, The Exchange–Correlation Effects on the Electronic Bands of Hybrid Armchair Single-Walled Carbon Boron Nitride Nanostructure, *Crystals*, 2022, **12**, 394.
7 S. I. Yahaya, B. S. Abdussalam, E. N. Chifu, L. Abdullahi and R. Razif, Computational Studies of the Excitonic and Optical Properties of Armchair SWCNT and SWBNNT for Optoelectronics Applications, *Crystals*, 2022, **12**, 870.
8 Y. S. Itas, E. N. Chifu and M. U. Khandaker, Synthesis of Thermally Stable h-BN-CNT Hetero-Structures via Microwave Heating of Ethylene under Nickel, Iron, and Silver Catalysts, *Crystals*, 2021, **11**, 1097.
9 E. A. Turhan, *et al*, Properties and applications of boron nitride nanotubes, *Nanotechnology*, 2022, **33**, 242001.

10 Y. S. Itas, A. S. Balarabe, E. Chifu and M. U. Khandaker, Effects of oxygen absorption on the electronic and optical properties of armchair and zigzag Silicon Carbide Nanotubes (SiCNTs), *Phys. Scr.*, 2023, **98**, 015824.

11 S. A. Yamusa and A. Shaari, First-principles Study on the Structural, Electronic, and Elastic Properties of Transition Metal Dichalcogenides, *Phys. Access*, 2023, **3**, 133.

12 Y. S. Itas, A. B. Suleiman, A. S. Yamusa, R. Razali and A. M. Danmadami, Ab initio studies of the structural and electronic properties for single-walled armchair MgONT, SiCNTs and ZnONTs for next generations' optoelectronics, *Gadau J. Pure. Alli. Sci.*, 2022, **1**, 160–165.

13 Y.-Q. Xu, S.-Y. Wu, J.-X. Guo, L.-N. Wu and L. Peng, First-principles investigation on the structural, elastic and electronic properties and mechanism on the photocatalytic properties for $SrNbO_3$ and $Sr_{0.97}NbO_3$, *J. Phys. Chem. Solids*, 2017, **111**, 403–409.

14 V. K. Choyal, V. Choyal, S. Nevhal, A. Bergaley and S. I. Kundalwal, Effect of aspects ratio on Young's modulus of boron nitride nanotubes: Aamolecular dynamics study, *Mater. Today*, 2020, **26**, 1–4.

15 K. M. Reza, A. S. W. Kurny and F. Gulshan, Parameters affecting the photocatalytic degradation of dyes using TiO_2: a review, *Appl. Water Sci.*, 2017, **7**, 1569–1578.

16 Y. S. Itas, A. B. Balarabe, E. N. Chifu and M. U. Khandaker, First-Principle Studies of the Structural, Electronic, and Optical Properties of Double-Walled Carbon Boron Nitride Nanostructures Heterosystem under Various Interwall Distances, *J. Chem.*, 2023, **2023**, 4574604.

17 Y. S. Itas, A. Baballe, A. M. Danmadami and S. A. Yahaya, Analysis of different welding speeds and the micro structure on the welded joints of silicon steel pipe, *IOP Conf. Ser.: Mater. Sci. Eng.*, 2020, **932**, 012123.

18 P. Li, Y. Lin, M. Ma, Q. Wang, M. Zhang and J. Li, Effect of pressure on photocatalytic water splitting performance of Z-scheme RP/CH3NH3PbI3 perovskite heterostructure, *Int. J. Hydrogen Energy*, 2022, **47**, 8091–8104.

19 Z. Hefeng, L. Jiaqi, X. Ting, J. Wenqian and Z. Xu, Recent Advances on Small Band Gap Semiconductor Materials ($\leq$2.1 eV) for Solar Water Splitting, *Catalysts*, 2023, **13**, 728.

20 Y. S. Itas, A. B. Suleiman, C. E. Ndikilar, A. Lawal, R. Razali and A. M. Danmadami, Effects of Ir and B co-doping on H2 adsorption properties of armchair carbon nanotubes using Optical Spectra Analysis for energy storage, *Gadau J. Pure. Alli. Sci.*, 2023, **2**, 30–39.

21 Y. S. Itas, B. S. Abdussalam, E. N. Chifu, R. Razif and A. Lawal, Dft Studies of Structural, Electronic and Optical Properties of (5, 5) Armchair Magnesium Oxide Nanotubes (Mgonts), *SSRN Electron. J.*, 2022, **2022**, 11.

22 Y. S. Itas, M. U. Khandaker and R. Razif, Studies of H2 storage efficiency of metal-doped carbon nanotubes by optical adsorption spectra analysis, *Diamond Relat. Mater.*, 2023, **136**, 109964.

23 Y. Saadu Itas, A. B. Suleiman and E. Chifu, Ndikilar, Abdullahi Lawal, Razif Razali & Mayeen Uddin Khandaker, "Effects of SiO2 and CO2 Absorptions on the Structural, Electronic and Optical Properties of (6, 6) Magnesium Oxide Nanotube (MgONT) for Optoelectronics Applications, *Silicon*, 2023, **2023**, 1–12.

24 T. Movlarooy, A. Kompany, S. M. Hosseini and N. Shahtahmasebi, Optical absorption and electron energy loss spectra of single-walled carbon nanotubes, *Comput. Mater. Sci.*, 2010, **49**, 450–456.

25 R. Pereira Cavalcante, R. Falcao Dantas, B. Bayarri, O. González, J. Giménez, E. Santiago and A. Machulek Jr, Photocatalytic mechanism of metoprolol oxidation by photocatalysts TiO2 and TiO2 doped with 5% B: primary active species and intermediates, *Appl. Catal., B*, 2016, **194**, 111–122.

26 J. O. Olowoyo, M. Kumar, S. L. Jain and J. O. Babalola, Insights into Reinforced Photocatalytic Activity of the CNT–TiO2 Nanocomposite for CO2 Reduction and Water Splitting, *J. Phys. Chem. C*, 2019, **123**, 367–378.

27 M. Irfan, S. Afzal, M. Hussain and M. Yasin Naz, Testing of Sr-Doped ZnO/CNT Photocatalysts for Hydrogen Evolution from Water Splitting under Atmospheric Dielectric Barrier Plasma Exposure, *ACS Omega*, 2023, **8**, 18891–18900.

28 Y. Huang, R. Li, D. Chen, X. Hu and P. Chen, Synthesis and Characterization of CNT/TiO2/ZnO Composites with High Photocatalytic Performance, *Catalysts*, 2018, **8**, 151.

29 A. Raveendran, M. Chandran and R. Dhanusuraman, A comprehensive review on the electrochemical parameters and recent material development of electrochemical water splitting electrocatalyst, *RSC Adv.*, 2023, **13**, 3843–3876.

30 D. C. d. Moura, M. A. Quiroz, D. Ribeiro da Silva, R. Salazar and C. Alberto Martínez-Huitle, Electrochemical degradation of Acid Blue 113 dye using TiO2-nanotubes decorated with PbO2 as anode, *Environ. Nanotechnol., Monit. Manage.*, 2016, **5**, 13–20.

31 V. Maheskumar, T. Selvaraju and B. Vidhya, Influence of solvent in solvothermal synthesis of Cu3SnS4: morphology and band gap dependant electrocatalytic hydrogen evolution reaction and photocatalytic dye degradation, *Int. J. Hydrogen Energy*, 2018, **43**, 22861–22873.

32 E. Kusmierek, Semiconductor Electrode Materials Applied in Photoelectrocatalytic Wastewater Treatment—an overview, *Catalysts*, 2020, **10**, 439.

33 N. R. Kumar, P. Das, A. R. Agrawal, S. K. Mandal and S. S. Zade, Thienyltriazine based conjugated porous organic polymers: tuning of the porosity and band gap, and CO2 capture, *Mater. Adv.*, 2021, **2**, 7473–7481.